# VSP modelling in 1D with Q and buried source

Gary F. Margrave and P.F. Daley


## SUMMARY

A published method for the calculation of 1D synthetic seismograms with constant-$Q$ attenuation is described and extended to the case of a VSP with a buried source. Based on layer matrices (or propagator matrices) the method is very accurate for a broad frequency range from low to high and efficiently models fine layering. Extensions to allow internal multiples, surface related multiples, and attenuation to be included or not, are described. The method runs rapidly (a minute or less) in native Matlab code even with thousands of layers. This is suitable to study the effect of internal multiples and attenuation on a synthetic seismogram. The method also has the ability to create both pressure and displacement responses making it suitable to studying geophone and hydrophone recordings. Examples from a simple conceptual model and from well logs are shown.


## INTRODUCTION

Seismic modelling for the case of a zero-offset *vertical seismic profile*, or VSP, is considered here as a generalization of the construction of a 1D normal incidence synthetic seismogram from well-log information. A common approach is that of Waters (1992) in which the well logs are "blocked" or resampled into layers of constant "time thickness" and then all reflection arrivals (primaries and multiples) are computed from a recursion. As presented in Waters, the method used a computational mesh to compute all possible primaries and multiples, with their respective transmission losses, but does not include anelastic attenuation. Also, both source and receiver are considered to be at the earth's surface which is either taken as the first logged depth or, with inclusion of a simple overburden model, as the surface elevation at the well. To generalize this to a VSP configuration, the solution must be generalized to allow any receiver depth.

The further generalizations considered here stem partially from the method of Ganley (1981) and are partially original. The solution is still 1D (so no wavefront spreading and no source offset) but inclusion of constant-$Q$ attenuation is directly modelled. Moreover, there is no resampling to layers of constant traveltime thickness and there is no need for the layers to have uniform depth thickness. The method, as coded in Matlab and released to CREWES Sponsors, is sufficiently efficient that models can be run at or near the depth sample rate of the logs (typically 1 ft) in just a few minutes on a personal computer. This allows the study of fine layering effects such as stratigraphic filtering (O'Doherty and Anstey, 1971) and described elsewhere in this research report (Margrave, 2014). Ganley's approach differs from earlier methods (e.g. Trorey, 1962) by the use of frequency-domain layer matrices instead of the computational mesh of Waters or Trorey. Such matrices automatically include all multiples, transmission losses, traveltime, and Q attenuation, and this greatly simplifies the algorithmic structure. Also, by working in the frequency domain, the frequency-dependent effects of attenuation can be faithfully modelled to very high frequencies. This is in contrast to some modern finite difference

approaches such as Emmerich and Korn (1987) or Krebes and Quiroga-Goode (1994) where considerable oversampling is required to reach high frequencies with fidelity.

Ganley's method easily generalizes to a receiver at any depth but arbitrary source depth is more complicated. While Ganley gave a solution for arbitrary source deopth, an alternative with clear physical foundation is given here. We also extend Ganley's method to model either pressure or displacement, and show how to turn on and off such effects as internal multiples, transmission losses, and attenuation.

## THEORY

### Layer matrices and their use

This development follows that of Ganley (1981) but is presented here in a revised manner. Here we describe the mathematical entities required for the construction of the layer matrices and show how they are used to extrapolate the wavefield solution up or down through the model. For each layer, there exists a propagator, $P_k$, to be defined explicitly later, that propagates a wavefield forward in time across the layer. If we define $D_k$ and $U_k$ to be the downgoing and upgoing wavefields at the top of the layer, then $P_k D_k$ and $P_k^{-1} U_k$ are the downgoing and upgoing waves at the layer bottom (Figure 1). The use of the inverse propagator is required on the upgoing wave since it must move backward in time to go from the top to the bottom of the layer.

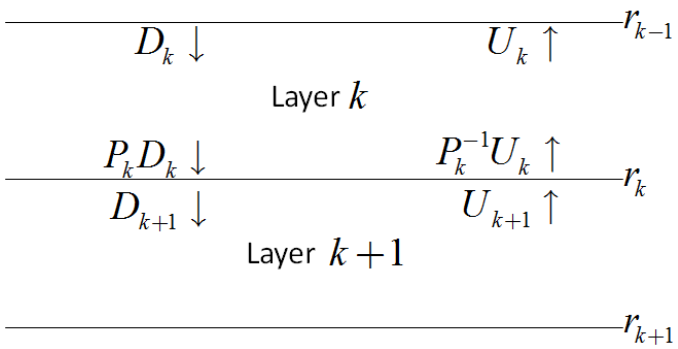


Figure 1: The waves and propagators used in the theory are depicted as they interact with interface $k$ where the reflection coefficient is $r_{k.}$ The downgoing and upgoing waves at the top of layer $k$ are $D_k$ and $U_k$ while at the top of layer $k+1$ they are $D_{k+1}$ and $U_{k+1}$. At the bottom of the same layer these waves are $P_k D_k$ and $P_k^{-1} U_k$ where $P_k$ describes propagation *forward in time* across the layer. The inverse propagator is needed on the upgoing wave at the bottom of the layer because that wavefield is earlier in time compared to the upgoing wave at the layer top. Waves $P_k D_k$ and $U_{k+1}$ are incident on interface $k$ while waves $P_k^{-1} U_k$ and $D_{k+1}$ are scattered from the interface. Equations 1 and 2 give the scattered waves in terms of the incident waves. Equation 6 uses the layer matrix (equation 5) to relate the waves at the top of layer $k$ to those at the top of layer $k+1$.

Let $r_k$ be the reflection coefficient for incidence from above at the $k^{\text{th}}$ interface and we take the $k^{\text{th}}$ layer to lie between interfaces $k$-1 and $k$. At the $k^{\text{th}}$ interface, the incident waves are $P_k D_k$ and $U_{k+1}$ which relate to the scattered waves $P_k^{-1} U_k$ and $D_{k+1}$ via

$$D_{k+1} = \underbrace{(1-r_k)P_k D_k}_{transmission} \underbrace{-Rr_k U_{k+1}}_{reflection} \tag{1}$$

and

$$P_k^{-1}U_k = \underbrace{Rr_k P_k D_k}_{reflection} \underbrace{+(1+r_k)U_{k+1}}_{transmission}, \tag{2}$$

where $R$ is -1 for a displacement solution and +1 for pressure. With some algebra, these equations can be re-arranged to give explicit formulae for $D_k, U_k$ in terms of $D_{k+1}, U_{k+1}$

$$D_k = \frac{P_k^{-1}}{1-r_k} D_{k+1} + \frac{Rr_k P_k^{-1}}{1-r_k} U_{k+1} \tag{3}$$

and

$$U_k = \frac{Rr_k P_k}{1-r_k} D_{k+1} + \frac{P_k}{1-r_k} U_{k+1}. \tag{4}$$

We define the *layer matrix* $\underline{\underline{A}}_k$ as

$$\underline{\underline{A}}_k = \frac{1}{1-r_k}\begin{bmatrix} P_k^{-1} & Rr_k P_k^{-1} \\ Rr_k P_k & P_k \end{bmatrix} \tag{5}$$

and then equations 3 and 4 can be combined into the matrix equation

$$\begin{bmatrix} D_k \\ U_k \end{bmatrix} = \underline{\underline{A}}_k \begin{bmatrix} D_{k+1} \\ U_{k+1} \end{bmatrix} = \begin{bmatrix} A_{k,11} & A_{k,12} \\ A_{k,21} & A_{k,22} \end{bmatrix} \begin{bmatrix} D_{k+1} \\ U_{k+1} \end{bmatrix}. \tag{6}$$

Layer matrices contain all physical effects including propagation, attenuation, transmission, reflection, and reverberation. Simple modifications of the layer matrix can be used to turn off selected physical effects. If it is desired to turn off internal multiples, then we must set all reflections of upgoing waves to zero. That is, we set the reflection term in equation 1 to zero. Some algebra then shows that the layer matrix is changed to

$$\underline{\underline{A}}_k^{\text{no\_int}} = \frac{1}{1-r_k}\begin{bmatrix} P_k^{-1} & 0 \\ Rr_k P_k & (1-r_k^2)P_k \end{bmatrix}. \tag{7}$$

If we further wish to suppress transmission losses (suppressing both internal multiples and transmission losses give the popular “primaries only” seismogram) then we must also set the transmission coefficients in equations 1 and 2 to unity. The result is a layer matrix which suppresses internal multiples and transmission losses given by

$$\underline{\underline{A}}_k^{\text{po}} = \begin{bmatrix} P_k^{-1} & 0 \\ Rr_k P_k & P_k \end{bmatrix}. \tag{8}$$

For the k[th] layer, the propagator is given by

$$P_k = e^{-\pi f h_k/(Q_k v_k)} e^{-i2\pi f h_k/v_k} \tag{9}$$

where $f$ is frequency, $h_k$ is the layer thickness, $Q_k$ is the attenuation constant for the layer, and $v_k$ is the frequency-dependent phase velocity. The assumed form for $v_k$ is

$$v_k = \frac{v_0}{1 - \frac{1}{\pi Q_k}\ln\left(\frac{f}{f_0}\right)} \approx v_0\left[1 + \frac{1}{\pi Q_k}\ln\left(\frac{f}{f_0}\right)\right], \tag{10}$$

where $v_0$ is the velocity at the reference frequency $f_0$. Justification for equations 9 and 10 may be found in Ganley (1981) or a seismology text such as Aki and Richards (2002). Essentially, these equations implement the constant-Q model of attenuation (e.g. Kjartanssen, 1979). In equation 10, we take $v_0$ to be the value measured in a sonic log which is typically done with a frequency, $f_0$, near 12500 Hz. Theory also requires that the reflection coefficients for incidence from above be calculated with the frequency-dependent phase velocity as

$$r_k = \frac{\rho_{k+1}v_{k+1} - \rho_k v_k}{\rho_{k+1}v_{k+1} + \rho_k v_k} \tag{11}$$

where $\rho_k$ is the layer density. Thus, in addition to frequency-dependent attenuation and phase delay caused by the propagator of equation 9, the constant Q model predicts frequency-dependent reflection via equation 11.

The form of equation 6 implies that the layer matrices can be composited to relate the solution in the first layer to that in the bottom half space by

$$\begin{bmatrix} D_1 \\ U_1 \end{bmatrix} = \underline{\underline{A}}_1\underline{\underline{A}}_2\cdots\underline{\underline{A}}_n\begin{bmatrix} D_{n+1} \\ U_{n+1} \end{bmatrix} = \underline{\underline{A}}\begin{bmatrix} D_{n+1} \\ U_{n+1} \end{bmatrix}, \tag{12}$$

where

$$\underline{\underline{A}} \equiv \prod_{k=1}^{n}\underline{\underline{A}}_k\,. \tag{13}$$

Generally we will assume $U_{n+1} = 0$ and relate $U_1$ and $D_1$ through a free surface condition. This reduces equation 12 to two equations in two unknowns and the solution is obtained. All of the entities in equation 12 are functions of frequency, so we must solve this equation independently for every frequency of interest. There is no constraint on the thicknesses or the properties of the layers used so we do not need the constant time-thickness layers or even constant depth thickness. It remains to specify the source.

**Case of source at the surface z=0**

This is the easiest case because we only consider a downgoing wave from the source. In the first layer, the downgoing and upgoing waves are related by the free-surface condition at the top of the layer. The total downgoing field consists of the injected source wavelet plus the reflection of the upgoing field from the free surface. We write this as

$$D_1 = W - Rr_0 U_1, \tag{14}$$

where, as before $R$ is -1 for a displacement solution and +1 for pressure, $r_0 = 1$ is the free-surface reflection coefficient for incidence from above, and $W$ is the source waveform. The presence of $R$ in equation 14 describes the essential condition at the free surface that, in the absence of a source, the total field, $U_1 + D_1$, vanishes for pressure and doubles for displacement.

With this specification, equation 12 becomes

$$\begin{bmatrix} W - Rr_0 U_1 \\ U_1 \end{bmatrix} = \underline{\underline{A}} \begin{bmatrix} D_{n+1} \\ 0 \end{bmatrix} = \begin{bmatrix} A_{11} & A_{12} \\ A_{21} & A_{22} \end{bmatrix} \begin{bmatrix} D_{n+1} \\ 0 \end{bmatrix} \tag{15}$$

where $U_{n+1} = 0$ has been assumed and $\underline{\underline{A}}$ is given by equation 13. Matrix equation 15 is two equations with two unknowns ($U_1$ and $D_{n+1}$). The solution is

$$D_{n+1} = \frac{W}{A_{11} + Rr_0 A_{21}} \tag{16}$$

and

$$U_1 = A_{21} D_{n+1}. \tag{17}$$

Equations 16 and 17 give a complete solution for the case of a surface source. A surface receiver will record the sum of $U_1$ and $D_1$ while a receiver at the top of layer k will record the sum of $U_k$ and $D_k$. Since $D_{n+1}$ and $U_{n+1}$ are now known, the solution at any layer top can be calculated similar to equation 12 using an appropriate product of layer matrices from layers *k* to *n*. Receivers inside a layer can be simulated by first computing the result at the layer top and then propagating it with a suitable propagator (modified from equation 9) to the actual receiver location.

**Case of source in first layer**

Consider a first layer, perhaps of considerable thickness, with the source located within it and divide that layer into two with an imaginary boundary at the source depth. Then call the portion of the layer above the source layer 1, and below the source as layer 2. The reflection coefficient at the interface of these layers is $r_1 = 0$ and the source is simultaneously at the bottom of layer 1 and at the top of layer 2. The upper surface of layer 1 is a free surface and this causes the downgoing and upgoing waves in that layer to be related to each other via

$$D_1 = -Rr_0 U_1 . \tag{18}$$

We now relate the downgoing and upgoing waves at the top of layer 1, $D_1, U_1$, to the corresponding waves at the top of layer 2. At the interface between these two layers, the source injects an upgoing wavelet $W_u$ and a downgoing wavelet $W_d$. Thus $D_2$ is the sum of $D_1$ propagated across layer 1 and $W_d$

$$D_2 = P_1 D_1 + W_d , \tag{19}$$

where $P_1$ describes the propagation of a downgoing wave down through layer 1 (or an upgoing wave up through layer 1). Similarly $U_1$ is the sum of $U_2$ and $W_u$ propagated up across layer 1

$$U_1 = P_1 \left( U_2 + W_u \right) . \tag{20}$$

Equations 19 and 20 are equivalent to

$$\begin{bmatrix} D_1 \\ U_1 \end{bmatrix} = \begin{bmatrix} P_1^{-1} & 0 \\ 0 & P_1 \end{bmatrix} \begin{bmatrix} D_2 - W_d \\ U_2 + W_u \end{bmatrix} . \tag{21}$$

Layers 2 through n have non-diagonal layer matrices and the wavefields in layer 2 can be related to those in the bottom half space below layer n by

$$\begin{bmatrix} D_2 \\ U_2 \end{bmatrix} = \underline{\underline{A}} \begin{bmatrix} D_{n+1} \\ 0 \end{bmatrix} = \begin{bmatrix} A_{11} & A_{12} \\ A_{21} & A_{22} \end{bmatrix} \begin{bmatrix} D_{n+1} \\ 0 \end{bmatrix} , \tag{22}$$

where

$$\underline{\underline{A}} = \prod_{k=2}^{n} \underline{\underline{A}}_k = \underline{\underline{A}}_2 \underline{\underline{A}}_3 \cdots \underline{\underline{A}}_n , \tag{23}$$

in which the $\underline{\underline{A}}_k$ are the layer matrices for the individual layers. (Note the slight difference between equations 23 and 13.)

We can describe the source wavelet in terms of a single waveform as

$$W_d = W , \tag{24}$$

and

$$W_u = RW . \tag{25}$$

The occurrence of $RW$ as the source term in equation 25, while in equation 24 we have just $W$, causes the upgoing and downgoing displacements to have opposite signs while the upgoing and downgoing pressures are equal, as is expected for an explosive source.

From 18, 19, 20, 24 and 25 we have

$$D_2 = -P_1 R r_0 U_1 + W\,, \tag{26}$$

$$U_2 = P_1^{-1} U_1 - RW\,. \tag{27}$$

Then combining these with 22 we have

$$A_{11} D_{n+1} = -P_1 R r_0 U_1 + W\,, \tag{28}$$

$$A_{21} D_{n+1} = P_1^{-1} U_1 - RW\,. \tag{29}$$

These are two equations for the unknowns $U_1$ and $D_{n+1}$. Substituting 29 into 28 gives

$$A_{11} D_{n+1} = -P_1 R r_0 \left( P_1 A_{21} D_{n+1} + P_1 RW \right) + W \tag{30}$$

so that

$$D_{n+1} \left( A_{11} + R r_0 P_1^2 A_{21} \right) = W \left( 1 - P_1^2 r_0 \right). \tag{31}$$

and finally

$$D_{n+1} = \frac{W \left( 1 - P_1^2 r_0 \right)}{A_{11} + R r_0 P_1^2 A_{21}}\,, \tag{32}$$

and

$$U_1 = P_1 \left( A_{21} D_{n+1} + RW \right). \tag{33}$$

Thus equations 32 and 33 give a complete solution to the VSP problem for a source buried in the first layer.

**Case of source in an arbitrary layer**

Suppose the source is in layer *s*. As before we break layer s into two at the source depth and suppose that there are now *n* layers over a half space and $1 \le s \le n$. Thus the source is simultaneously at the bottom of layer *s* and the top of layer *s*+1. Then define

$$\underline{\underline{A}} = \prod_{k=s+1}^{n} \underline{\underline{A}}_k = \underline{\underline{A}}_{s+1} \underline{\underline{A}}_{s+2} \cdots \underline{\underline{A}}_n\,, \tag{34}$$

as the layer propagator connecting the half-space with layer s+1, and

$$\underline{\underline{B}} = \prod_{k=1}^{s-1} \underline{\underline{A}}_k = \underline{\underline{A}}_1 \underline{\underline{A}}_2 \cdots \underline{\underline{A}}_{s-1}\,, \tag{35}$$

as the propagator connecting layer s with layer 1. (Layer s occurs in neither $\underline{\underline{A}}$ or $\underline{\underline{B}}$.) Similar to equation 21, the fields in layers *s* and *s*+1 are related by

$$\begin{bmatrix} D_s \\ U_s \end{bmatrix} = \begin{bmatrix} P_s^{-1} & 0 \\ 0 & P_s \end{bmatrix} \begin{bmatrix} D_{s+1} - W \\ U_{s+1} + RW \end{bmatrix}, \tag{36}$$

while layer 1 relates to layer $s$ via

$$\begin{bmatrix} D_1 \\ U_1 \end{bmatrix} = \begin{bmatrix} B_{11} & B_{12} \\ B_{21} & B_{22} \end{bmatrix} \begin{bmatrix} D_s \\ U_s \end{bmatrix}, \tag{37}$$

and layers $n+1$and $s+1$ are related by

$$\begin{bmatrix} D_{s+1} \\ U_{s+1} \end{bmatrix} = \begin{bmatrix} A_{11} & A_{12} \\ A_{21} & A_{22} \end{bmatrix} \begin{bmatrix} D_{n+1} \\ 0 \end{bmatrix}. \tag{38}$$

Finally, the up and downgoing fields in layer 1 are linked by the free surface condition

$$D_1 = -Rr_0 U_1 . \tag{39}$$

From equation 37, we write

$$-Rr_0 U_1 = B_{11} D_s + B_{12} U_s , \tag{40}$$

$$U_1 = B_{21} D_s + B_{22} U_s , \tag{41}$$

and from equation 38

$$D_{s+1} = A_{11} D_{n+1}, \tag{42}$$

$$U_{s+1} = A_{21} D_{n+1}, \tag{43}$$

and from equation 36

$$D_s = P_s^{-1} \left( D_{s+1} - W \right), \tag{44}$$

$$U_s = P_s \left( U_{s+1} + RW \right). \tag{45}$$

From 45 and 43 we have

$$U_s = P_s A_{21} D_{n+1} + P_s RW \tag{46}$$

and from 44 and 42

$$D_s = P_s^{-1} \left( A_{11} D_{n+1} - W \right). \tag{47}$$

Now use 46 and 47 to eliminate $D_s$ and $U_s$ from 40 and 41 to get

$$-Rr_0 U_1 = B_{11} P_s^{-1} \left( A_{11} D_{n+1} - W \right) + B_{12} \left( P_s A_{21} D_{n+1} + P_s RW \right) \tag{48}$$

and

$$U_1 = B_{21}P_s^{-1}\left(A_{11}D_{n+1} - W\right) + B_{22}\left(P_s A_{21}D_{n+1} + P_s RW\right). \qquad (49)$$

Equations 48 and 49 are two equations for the two unknowns $U_1$ and $D_{n+1}$. Eliminating $U_1$ gives

$$-Rr_0\left[B_{21}P_s^{-1}\left(A_{11}D_{n+1} - W\right) + B_{22}\left(P_s A_{21}D_{n+1} + P_s RW\right)\right] = B_{11}P_s^{-1}\left(A_{11}D_{n+1} - W\right) + B_{12}\left(P_s A_{21}D_{n+1} + P_s RW\right)$$

or

$$-Rr_0\left[B_{21}P_s^{-1}\left(A_{11}D_{n+1} - W\right) + B_{22}\left(P_s A_{21}D_{n+1} + P_s RW\right)\right] = B_{11}P_s^{-1}\left(A_{11}D_{n+1} - W\right) + B_{12}\left(P_s A_{21}D_{n+1} + P_s RW\right)$$

$$\left[-Rr_0B_{21}P_s^{-1}A_{11} - Rr_0B_{22}P_sA_{21} - B_{11}P_s^{-1}A_{11} - B_{12}P_sA_{21}\right]D_{n+1} = \left[-Rr_0B_{21}P_s^{-1} + r_0B_{22}P_s - B_{11}P_s^{-1} + B_{12}P_sR\right]W$$

So that

$$D_{n+1} = \frac{\left[B_{11} + Rr_0B_{21} - P_s^2\left(r_0B_{22} + B_{12}R\right)\right]W}{A_{11}\left(B_{11} + Rr_0B_{21}\right) + A_{21}P_s^2\left(B_{12} + Rr_0B_{22}\right)} \underset{\substack{B\to I\\ P_s\to P_1}}{=} \frac{\left[1 - r_0P_1^2\right]W}{A_{11} + Rr_0P_1^2A_{21}}, \qquad (50)$$

where the final limit shows agreement with the previous case in which the source is in the top layer.

We can write a form of equation 50 that suppresses surface related multiples by setting $r_0 = 0$. This results in

$$D_{n+1} = \frac{\left[B_{11} - P_s^2B_{12}R\right]W}{A_{11}B_{11} + A_{21}B_{12}P_s^2}. \qquad (51)$$

**Relationship between the buried source and surface source solutions**

There is a fundamental disconnect between the surface source expression for $D_{n+1}$ given by equation 16, and either buried source expression given by equation 32 or equation 50. The problem is that the surface source expression is not a limiting case of the buried source as the depth of burial goes to zero. Considering equation 32 we can see that, when the depth of burial goes to zero, $D_{n+1}$ vanishes. Intuitively, this is because the surface ghost and the downgoing primary cancel. From a physical perspective, we are familiar with explosive sources (dynamite on land and air guns in water) always being buried. Placing them at the surface would result in the vast majority of the energy being released to the atmosphere. On land, we have the Vibroseis source at the surface but it comes with a large hold-down weight which locally changes the boundary conditions beneath the machine to other than a free surface. Given these considerations, it is justifiable to treat these two theories (surface source and buried source) as distinct and maintain separate codes for each. In the CREWES library, the surface source is found as *vspmodelq* while the buried source is *vspmodelqs*.

**Extrapolation to the receiver**

The solution at any receiver can be found by extrapolating $D_{n+1}$ up to the receiver depth using an appropriate concatenation of layer matrices. (We could equally well choose to extrapolate $U_1$ down to the receiver depth.) However, we must use a slightly different form for the solution depending upon whether the receiver is above or below the source. We consider the most general case of the source in an arbitrary layer here with $D_{n+1}$ given by equation 50. Suppose the receiver is at the top of layer $r$, where $1 \le r \le n$, then, let

$$\underline{\underline{A}}^{r,n} = \prod_{k=r}^{n} \underline{\underline{A}}_k = \underline{\underline{A}}_r \underline{\underline{A}}_{r+1} \cdots \underline{\underline{A}}_{n-1} \underline{\underline{A}}_n \tag{52}$$

and

$$\underline{\underline{B}}^{r,s} = \prod_{k=r}^{s} \underline{\underline{A}}_k = \underline{\underline{A}}_r \underline{\underline{A}}_{r+1} \cdots \underline{\underline{A}}_{s-1} \underline{\underline{A}}_s, \quad r \le s\,. \tag{53}$$

As defined, $\underline{\underline{A}}^{r,n}$ represents propagation from the bottom layer up to the receiver, while $\underline{\underline{B}}^{r,s}$, defined only if the receiver is above the source, represents propagation from the source up to the receiver.

Then the solution at the receiver is given by

$$\begin{bmatrix} D_r \\ U_r \end{bmatrix} = \underline{\underline{A}}^{r,n} \begin{bmatrix} D_{n+1} \\ 0 \end{bmatrix}, \text{ for } r > s \text{ (receiver below source)} \tag{54}$$

and

$$\begin{bmatrix} D_r \\ U_r \end{bmatrix} = \underline{\underline{A}}^{r,n} \begin{bmatrix} D_{n+1} \\ 0 \end{bmatrix} - \underline{W}_{d,r} + \underline{W}_{u,r}, \text{ for } r < s \text{ (receiver above source)} \tag{55}$$

with

$$\underline{W}_{d,r} = \underline{\underline{B}}^{r,s} \begin{bmatrix} W \\ 0 \end{bmatrix} \tag{56}$$

and

$$\underline{W}_{u,r} = \underline{\underline{B}}^{r,s} \begin{bmatrix} 0 \\ RW \end{bmatrix}. \tag{57}$$

The extra terms in equation 55, as defined by equations 56 and 57, have an interesting physical interpretation. $\underline{W}_{d,r}$ is the downgoing source wavefield above the source level. This exists mostly in negative time and is present in the solution computed as in equation 54 because the method of defining the source (equation 36) lacks a causality condition.

That is, the downgoing source wavelet should not exist before time zero, but to enforce this we must calculate this term and subtract it. $\underline{W}_{u,r}$ is the upgoing direct wave from the source. This is also not contained in equation 54 and must be calculated explicitly.

## A SIMPLE SYNTHETIC EXAMPLE

To illustrate this theory and the resulting MATLAB code, consider the model shown in Figure 2. This model has physical interfaces at depths 200m, 750m, and 1350m, and is sampled at 10m. This means that there are 200 distinct layers each characterized by its own layer matrix $\underline{\underline{A}}_k$, $k \in [1, 200]$.

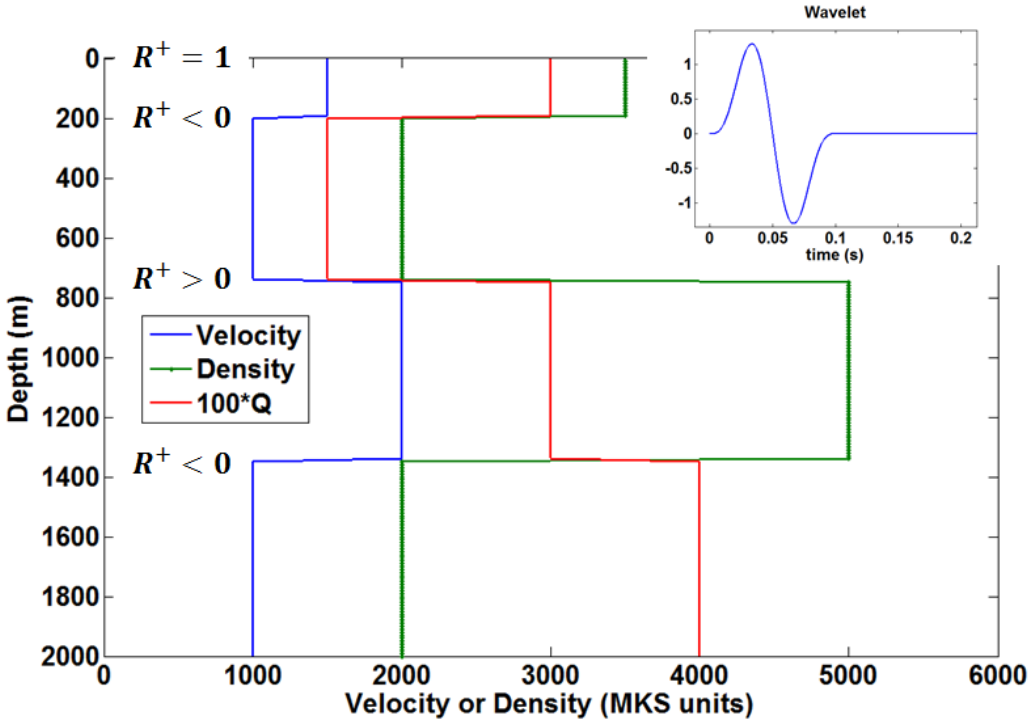


Figure 2: A simple 4-layer model. Curves are shown for velocity (m/s), density (kg/m$^3$), and Q (multiplied by 100). There are 4 physical layers but the model is sampled at 10m intervals so there are 200 numerical layers. The wavelet is also shown.

The displacement field resulting from this model is shown in Figure 3 where the source has been placed at a depth of 300 m which puts it just beneath the first physical interface. In this case, receivers were placed every 10m from 0 to 1500m. Also shown are layer interface positions, and events labelled A,B,C,D, which are respectively: the upgoing direct wave, the downgoing direct wave, the reflection of A from the free surface, and the reflection of B from the second interface. The upgoing and downgoing direct waves have opposite polarities as is expected for a displacement field from a compressional source. Also, event A preserves its polarity upon reflection from the free surface which results in a doubling of the displacement at the free surface. Conversely, event B reverses polarity upon reflection from the second interface. The different polarity behaviour of these two reflections is determined by the different impedance contrasts at the free surface and the second interface.

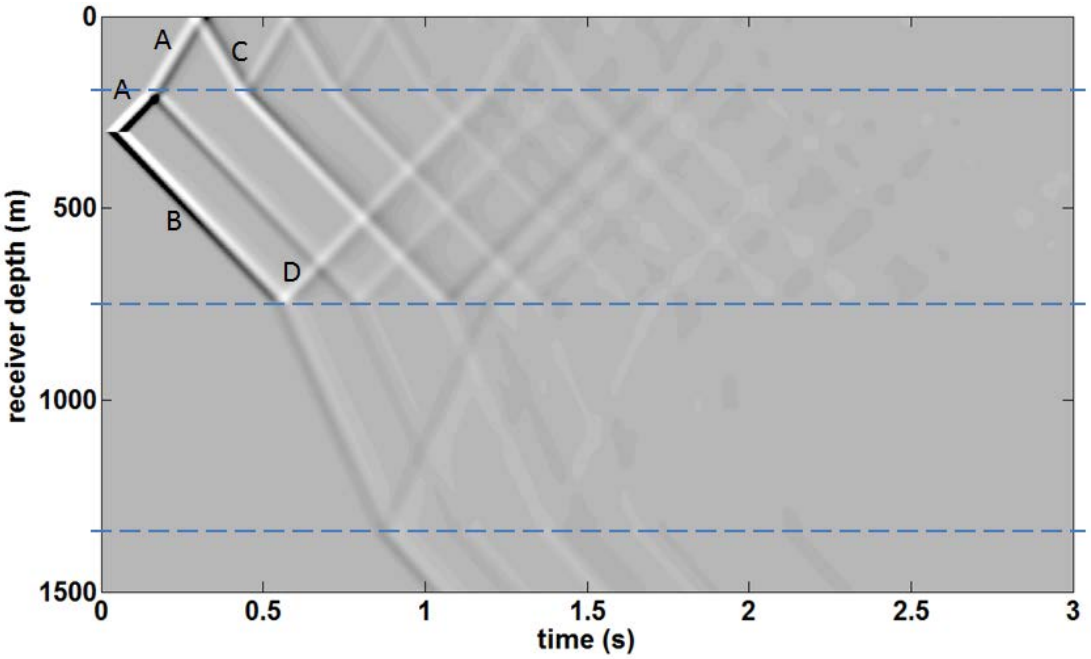


Figure 3: The total displacement field for the model of Figure 2. Below the source, the solution follows from equation 54 while above the source equation 55 is used. The horizontal dashed blue lines denote the physical interfaces in the model. The source is at 300m depth at the intersection of events A and B. Labeled events are A: The upgoing wave from the source; B: The downgoing wave from the source; C: The reflection of A from the free surface; D: The reflection of B from the second interface.

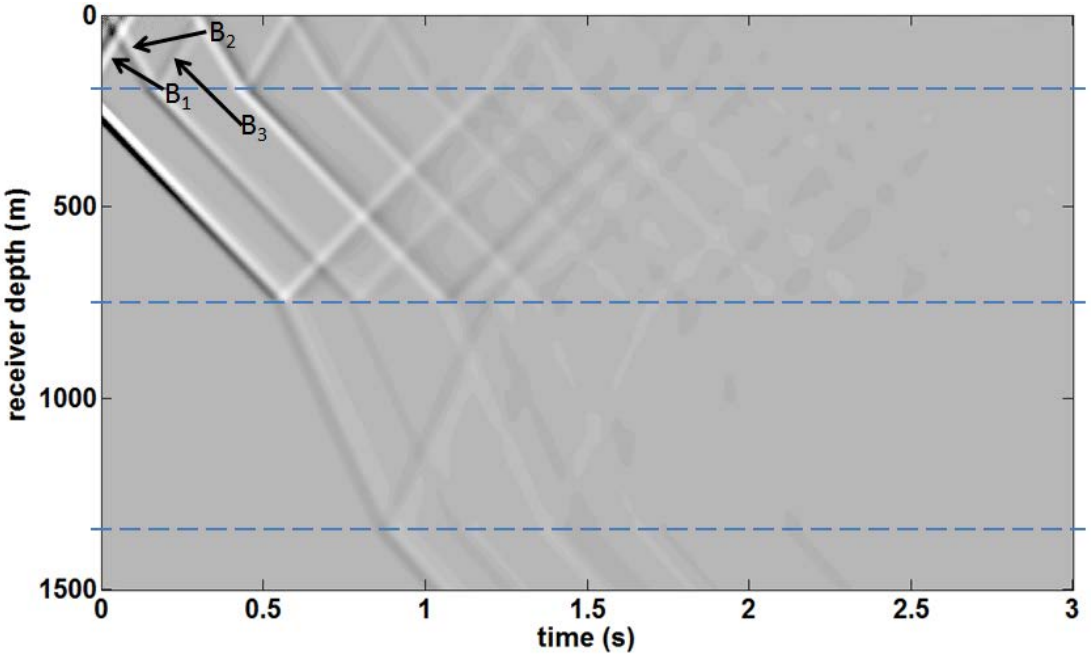


Figure 4: Similar to Figure 3 except that equation 54 is used both above and below the source. This illustrates the effect of the correction terms in equation 55. Labelled evens are $B_1$: The upgoing reflection of the downgoing direct wave when it encounters the first interface in negative time; $B_2$: The "ghost" reflection of the downgoing direct wave in negative time; $B_3$: The reflection of $B_2$ at the first interface.

Shown in Figure 4 is the displacement solution for this model when equation 54 is used both above and below the receiver. This illustrates the effect of the extra terms in equation 55. An enlarged comparison is found in Figure 5. As can be seen, the use of equation 54 above the source causes the downgoing direct wave to be unphysically extended above the source into negative time and omits the upgoing direct wave. This creates a series of unphysical events as this wave encounters interfaces and the free surface. Noise is also created (visible in the upper left of figure 5b) caused because the extension of the direct wave into negative time requires an inverse Q operator which rapidly overwhelms the dynamic range of the computation.

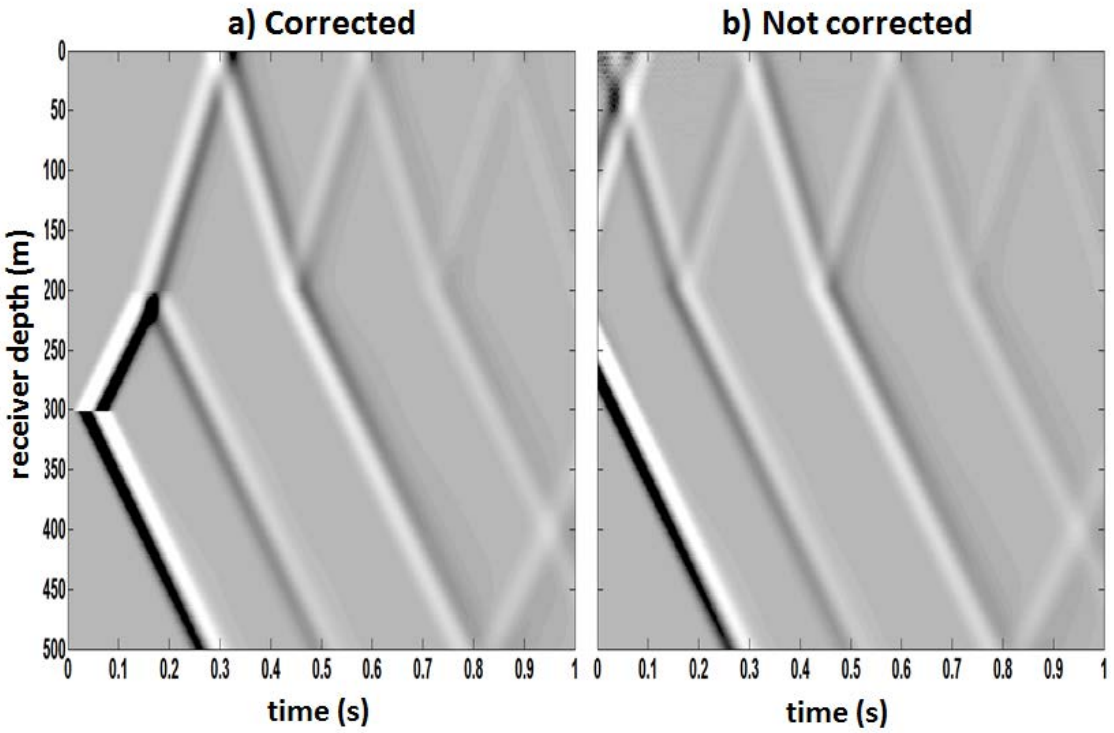


Figure 5: Enlargements of (a) the upper left corner of Figure 3 and (b) the upper left corner of Figure 4. This illustrates the effect of the extra terms in equation 55 that are needed above the source location. The source is at depth 300m. a) is the correct solution using both equations 54 and 55 while b) uses only equation 54 and is incorrect above the source.

## COMPARISON OF DISPLACEMENT AND PRESSURE SOLUTIONS

In the preceding theory (e.g. equation 50), the variable $R$ is -1 for a displacement solution and +1 for pressure. This allows the generation of either a 1D displacement solution or a pressure solution. In either case, the specified wavelet is also assumed to be specified in either displacement or pressure so that the resulting seismograms will not have scaling differences. However, they will have many phase (polarity) differences. Figure 6 is a side-by-side comparison of the displacement and pressure solutions for the model of Figure 2. In Figure 6, horizontal grey lines denote the depths of the three model interfaces (200m, 750m, and 1350m) while the vertical dotted lines are simply timing markers at 0.5 sec intervals. Aside from the obvious polarity differences of the upgoing direct wave as it leaves the source (source depth is 300m), there are also notable

differences in the polarity of reflections at the model interfaces and at the free surface (0m depth).

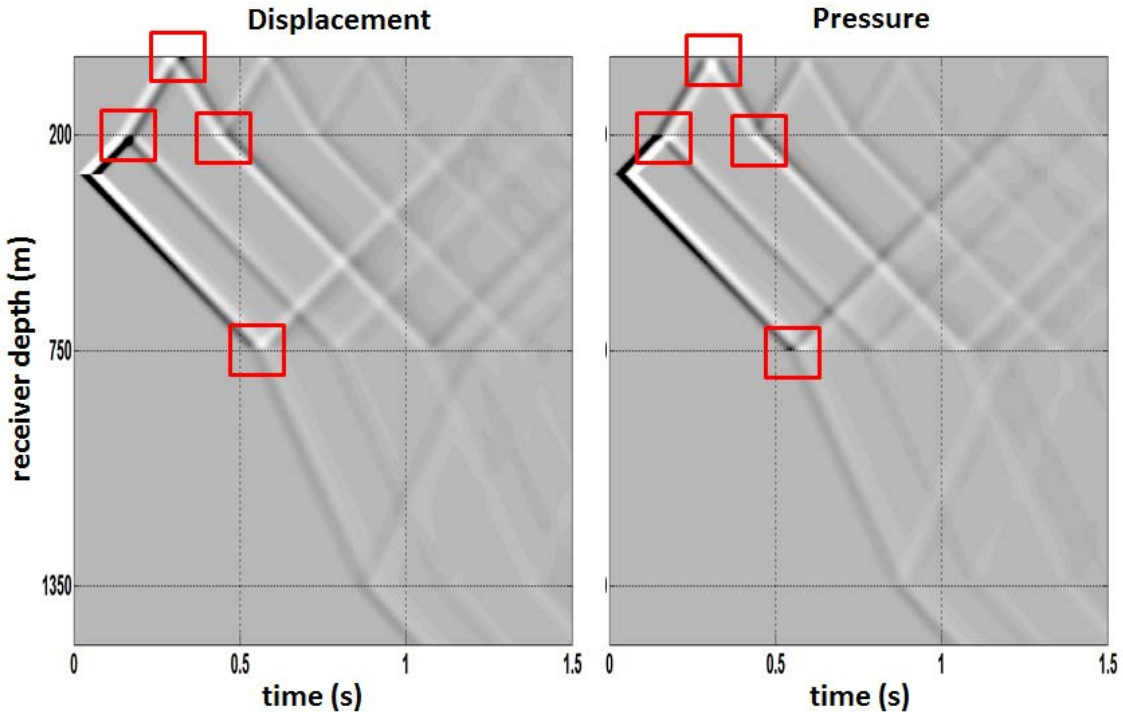


Figure 6: Comparison of the displacement solution (left) and the pressure solution (right) for the model of Figure 2. The source was at 300m depth. The red squares indicate areas shown enlarged in Figure 7.

To better understand these differences, it is useful to consider two extreme cases: that of incidence from below on a free surface, and that of incidence from above on a perfectly rigid medium. For any interface, we take the conventional definition of reflection coefficient for incidence from above as

$$r^+ = \frac{I_2 - I_1}{I_2 + I_1} \tag{58}$$

where $I_1$ is the impedance (density times velocity) above the interface, $I_2$ is the impedance below, and the + superscript indicates incidence from above. Defined in this way, if the lower medium has higher impedance than the upper then $r^+ > 0$, and vice-versa. For incidence from above, a displacement wave reflects according to

$$u_{ref} = -r^+ u_{inc} \tag{59}$$

while a pressure wave reflects as

$$p_{refl} = r^+ p_{inc}\,. \tag{60}$$

For incidence from below, we would use $r^- = -r^+$ in equation 59 and 60. These results are not meant to be obvious but they are standard results from textbooks in basic

seismology or acoustics. The derivation of these expressions assumes that both displacement and pressure must be continuous across the interface. The − sign in equation 59 means that, when $r^+ > 0$, then displacement reverses polarity on reflection while pressure does not. When $r^+ < 0$ then pressure reverses polarity on reflection while displacement does not. For the case of incidence from below, the reflection coefficient changes sign (i.e. $r^- = -r^+$) so that just the opposite set of polarity reversals occurs. Since transmission coefficients are always non-negative, there are no polarity reversals on transmission. Let us now see how this perfectly represents the two extreme cases.

First, for incidence from below on a free surface such as we have in our model at z=0, we intuitively expect that the total pressure must vanish at the interface because it must vanish in the vacuum above the interface and it must be continuous across the interface. Since $I_1 = 0$ in this case, we have $r^+ = 1$ and $r^- = -1$. Using $r^-$ in equation 60 we have $p_{refl} = -p_{inc}$ so that the total pressure at the interface ($p_{refl} + p_{inc}$) is zero. For displacement, we use $r^-$ in equation 59, to conclude $u_{ref} = u_{inc}$ so that the total displacement at the interface ($u_{ref} + u_{inc}$) is twice that of the incident wave. We can generalize these observations to the statement:

*For a wave incident from below when $r^+ > 0$, or for a wave incident from above when $r^+ < 0$, then pressure changes sign on reflection while displacement does not.*

Second, consider incidence from above on a perfectly rigid medium. This means that $I_2 \to \infty$ and $r^+ \to 1$. Since a perfectly rigid medium cannot have any motion, we expect that the total displacement must vanish at the interface because displacement must be continuous across the interface. Putting $r^+ = 1$ into equation 59 gives $u_{ref} = -u_{inc}$ so the total displacement does indeed vanish. Considering equation 60 in this context we see that the pressure at the boundary must be twice that of the incident wave. We then generalize to the following statement

*For a wave incident from above when $r^+ > 0$, or for a wave incident from below when $r^+ < 0$, then displacement changes sign on reflection while pressure does not.*

Careful inspection of Figure 6 shows instances of all of these situations. Figure 7 shows enlarged views of four different interactions. Panels a) and b) show the interaction with the free surface where the vanishing of total pressure and the doubling of displacement are easily apparent. Panels c) and d) show the upgoing direct wave interacting with the interface at 200m for which $r^+ < 0$. The polarity reversal of the reflected displacement is observable as is the non-reversal of the pressure wave. (Note that polarity is a property of the time series and must be assessed on these plots by scanning horizontally at constant depth.) Panels e) and f) show the downgoing reflection from the free surface interacting with the same 200m interface as the previous two panels. In this case incidence is from above and displacement does not reverse polarity while pressure does. Finally, panels g) and h) show the downgoing direct wave

interacting with the 750m interface for which $r^+ > 0$. In this case, displacement reverses polarity which pressure does not.

Further inspection of Figure 6 shows two events which might be considered as ghosts of the downgoing wave for the buried source. Both are reflections of the upgoing direct wave with the first ghost reflecting from the 200m interface and the second from the free surface. Careful comparison of the displacement and pressure solutions shows that the downgoing direct wave and the two ghosts are identical for both solutions. Further, we notice that the upgoing primary reflections of the two solutions are opposite in polarity.

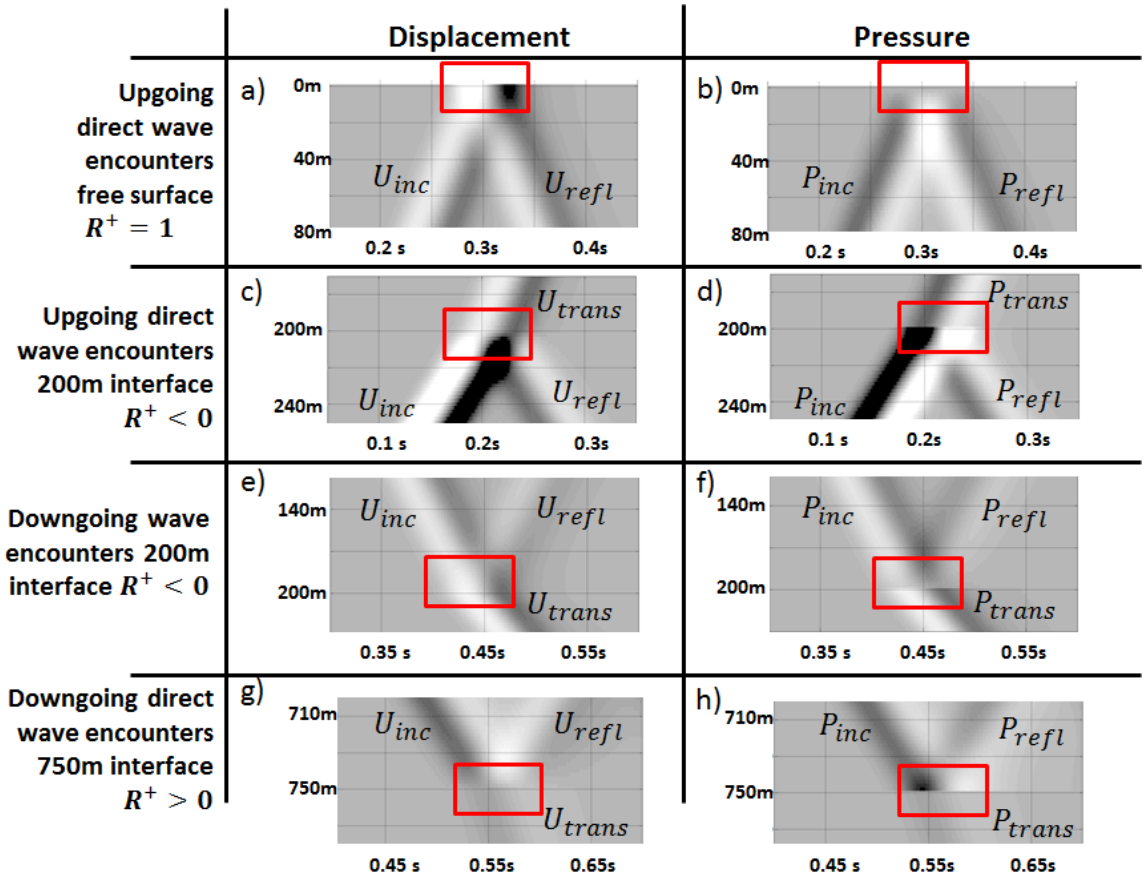


Figure 7: Enlargements of the areas indicated on Figure 6 allowing detailed comparison of the polarity differences between the displacement and pressure solutions. Here the red squares indicate the precise position of the interface.

## THE SOURCE GHOST AND THE P-Z SUBTRACTION TECHNIQUE

In the model of Figure 2, the upgoing direct wave from the source generates downgoing reflections at the 200m interface and at the free surface. Both of these events could be called source ghosts and both are highlighted, together with the downgoing direct wave, on Figure 8, which shows both the displacement and pressure solutions. The polarities of the direct wave and its ghosts are the same on both the displacement and pressure solutions; however, inspection shows that the various upgoing waves in the displacement solution are opposite in polarity to the same waves in the pressure solution. This is in fact generally true and is a consequence of equations 59 and 60. These basic

relations gave rise to the P-Z subtraction method (Barr and Sanders, 1989) who proposed to record both hydrophones (pressure) and geophones (particle velocity which is the time derivative of displacement) one the ocean bottom and, with some data processing involved, subtract the geophone recording from the hydrophone recording to eliminate the downgoing waves.

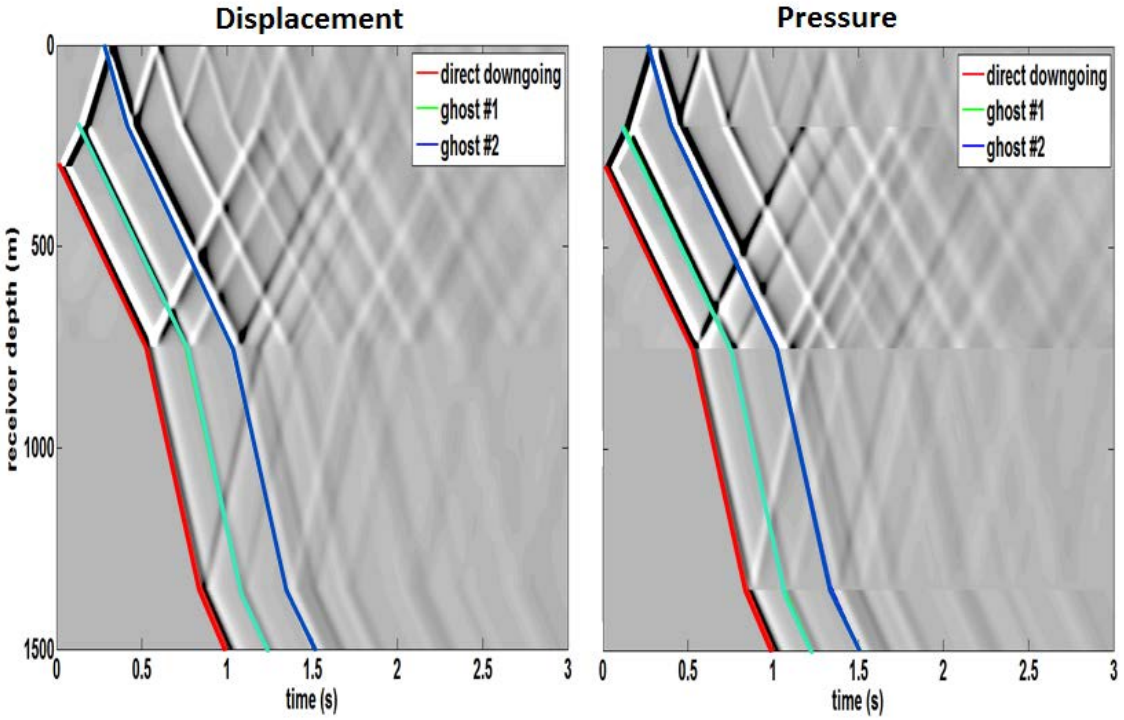


Figure 8: The pressure and displacement solutions for the model of Figure 2 are compared with the direct downgoing wave and its two phosts highlighted. The polarity of the downgoing waves are identical on both solutions while the upgoing pressure waves have polarity opposite to displacement.

Figure 9 shows the result of subtracting the displacement solution of Figure 8 from the pressure solution. In actual data processing, this step requires the estimation of a balancing filter that compensates for the different responses of hydrophones and geophones. However, this is not necessary with the present modelling code and the subtraction perfectly isolates the upgoing waves. Inspection of Figure 9 shows that the upgoing waves consist of primary reflections as well as reflections of the ghost waves and other downgoing waves.

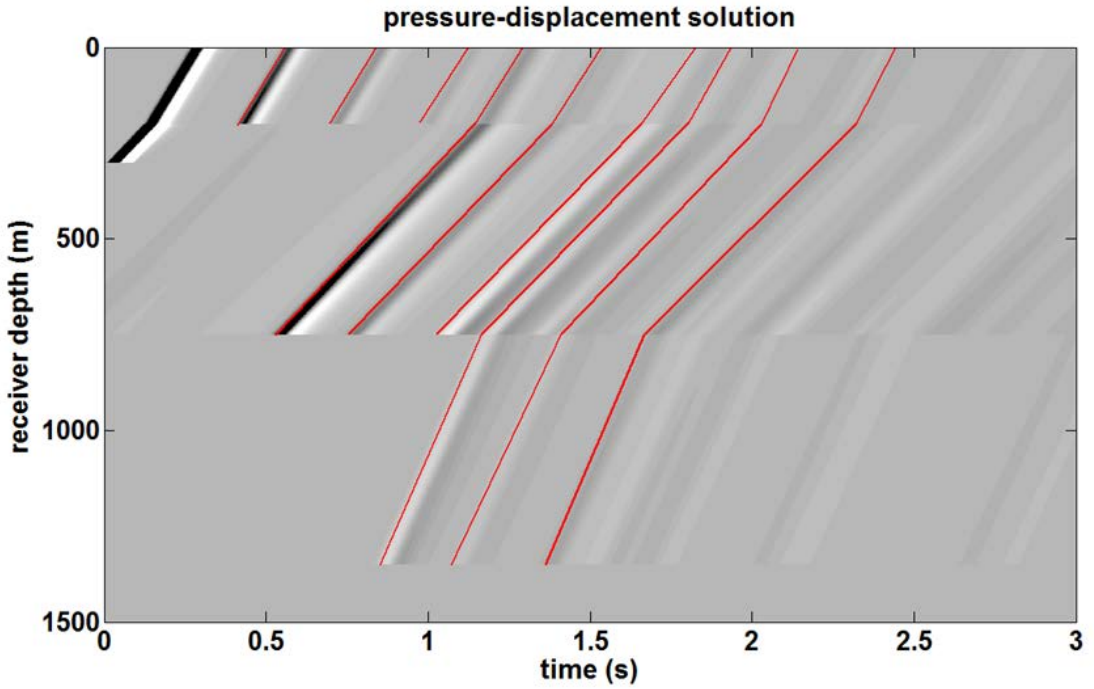


Figure 9: The result of subtracting the displacement field of Figure 8 from the pressure field. The downgoing waves have been eliminated and only the upgoing waves remain. The red lines indicate some of the upgoing events.

## AN EXAMPLE FROM WELL LOGS

The theory presented here places no restrictions on the number of layers in the model or their thicknesses. The most detailed descriptions of earth properties available to us are made in well logging experiments where typically measurements are made at 1 foot intervals. In Figure 10, an earth model is shown derived from Alberta well 1409 at Blackfoot field. The Q values were deduced from an empirical rule presented in Margrave (2013). The model shown is sampled at 1m intervals and was derived by resampling the well measurements with appropriate anti-alias averaging. Also shown is the 30 Hz dominant frequency, minimum-phase, wavelet used in the simulations which follow.

Figures 11, 12, and 13 show the displacement solutions for total field, downgoing field, and upgoing field for a source at z=0. Clearly these solutions are much more complex than the previous model because the layer properties have tremendous variation and because there are many more layers. Since the depth sample size is 1m, there are about 1700 total layers with the upper 200 layers having simple overburden properties while the lower 1500 layers have properties from the well logs. The Matlab code that implements this method runs in less than 1 minute on a modern PC. The rapidly fluctuating layer properties give rise to a complex pattern of reflection and transmission. Since the algorithm described here computes the upgoing and downgoing fields separately, we can easily display them and this helps in the interpretation of the results.

The next six figures show two buried source solutions for comparison with Figures 11-13. In Figures 14-16 are the total, downgoing, and upgoing fields for a source at

z=100m which is in the overburden. The source ghost from the free surface is clearly disable and lags about 200ms behind the primary downgoing wave. Comparing figures 13 and 16 shows that there are many more strong reflections in the case of the buried source than for the surface source. Figures 17-19 are the total, downgoing, and upgoing fields for a source at z=400m which is in the upper portion of the logged model. Now there are many more ghost reflections generated as the upgoing direct wave traverses the logged portion of the model between 400m and 200m. There are subtle horizontal lineations visible in some of these images (e.g. Figures 18 and 19 near 480m) and these correspond to low impedance zones in the model which produce large displacements.

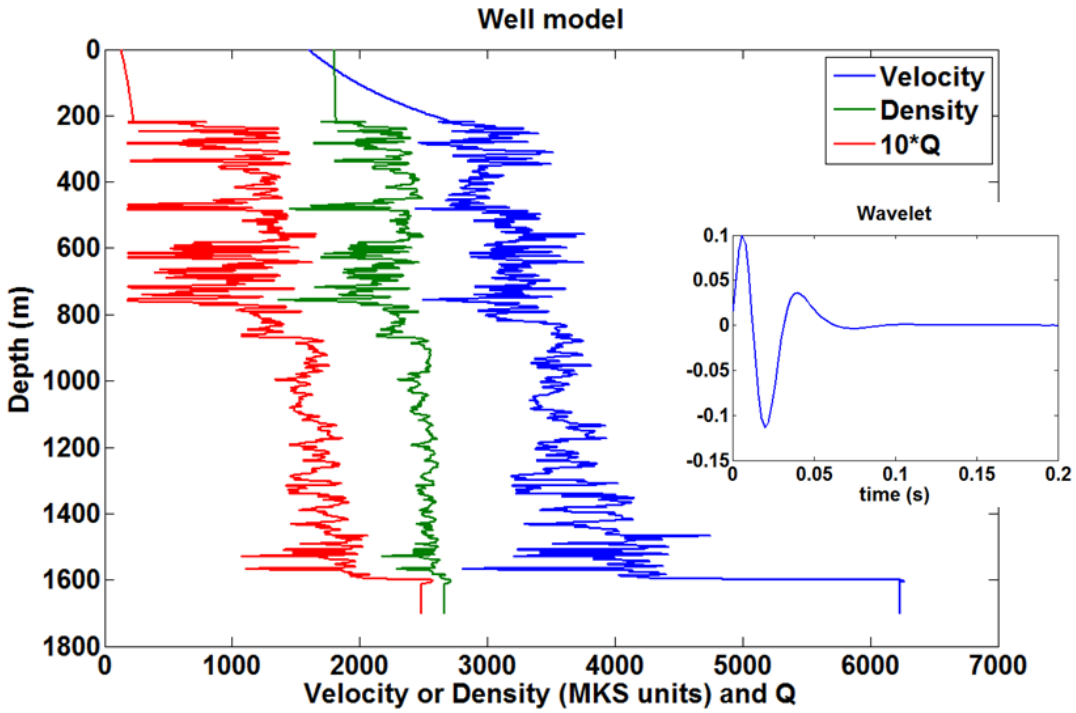


Figure 10: An earth model derived from well 1409 at Blackfoot field (Alberta). The original well was sampled at 1 ft intervals while the model shown here has been resampled to 1m. Curves for velocity and density come directly from measured values while the Q curve is deduced from the other two by an empirical rule. Logging started at 200m depth and an overburden model is shown to connect logged values to the surface. Also shown is the wavelet used in subsequent simulations.

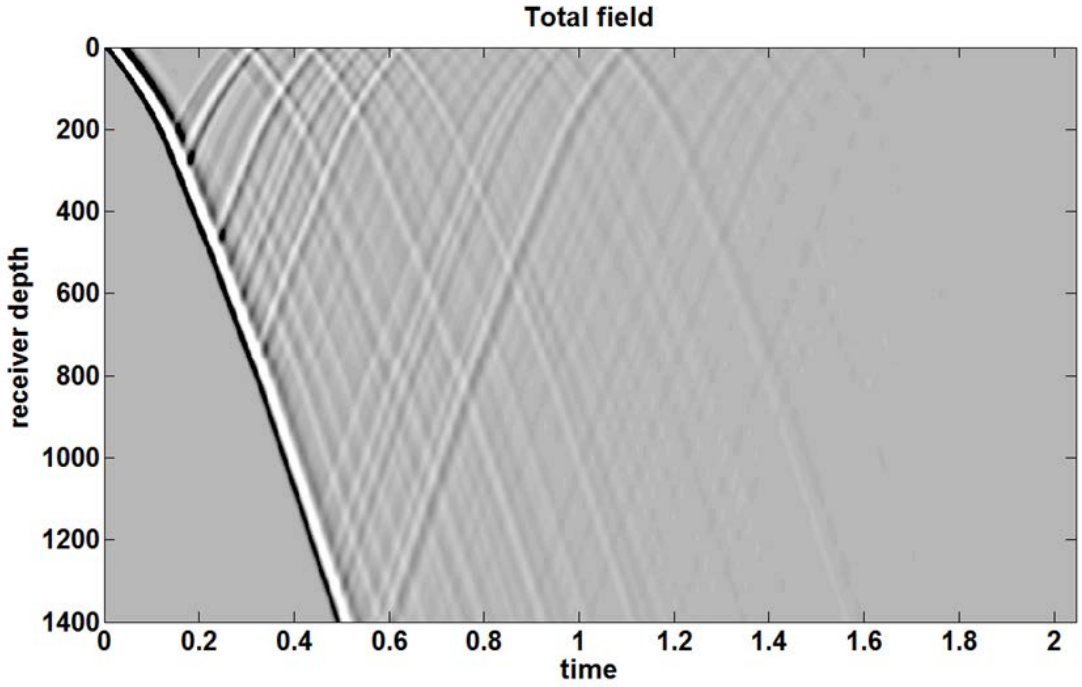


Figure 11: The total displacement field for the model of Figure 10 for a surface source (z=0).

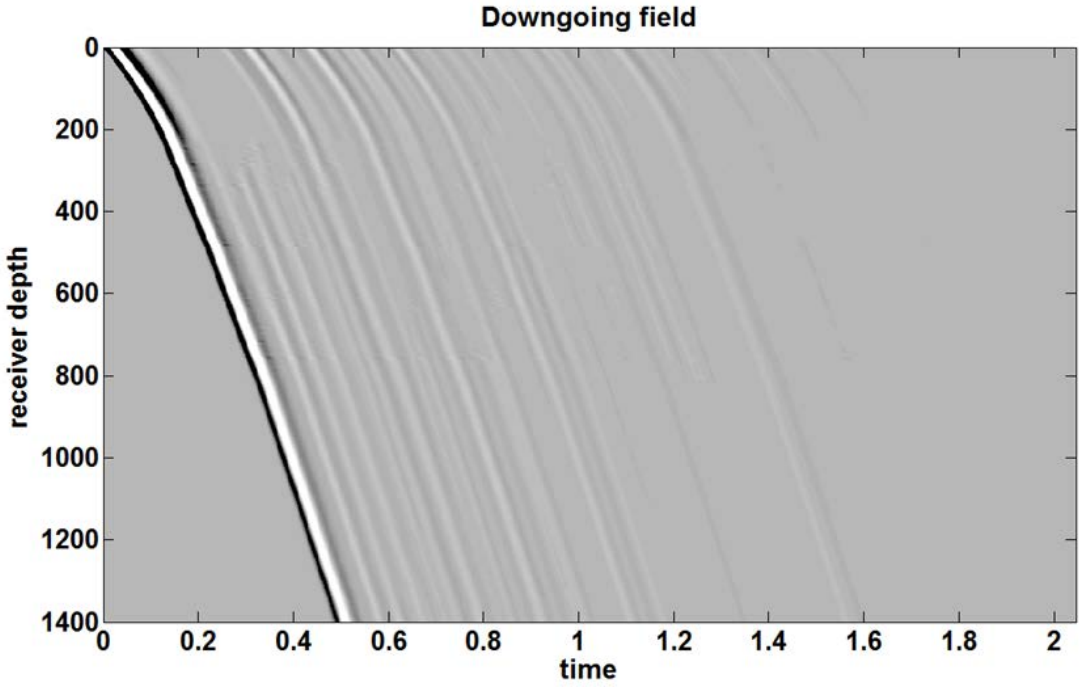


Figure 12: The downgoing field from Figure 11.

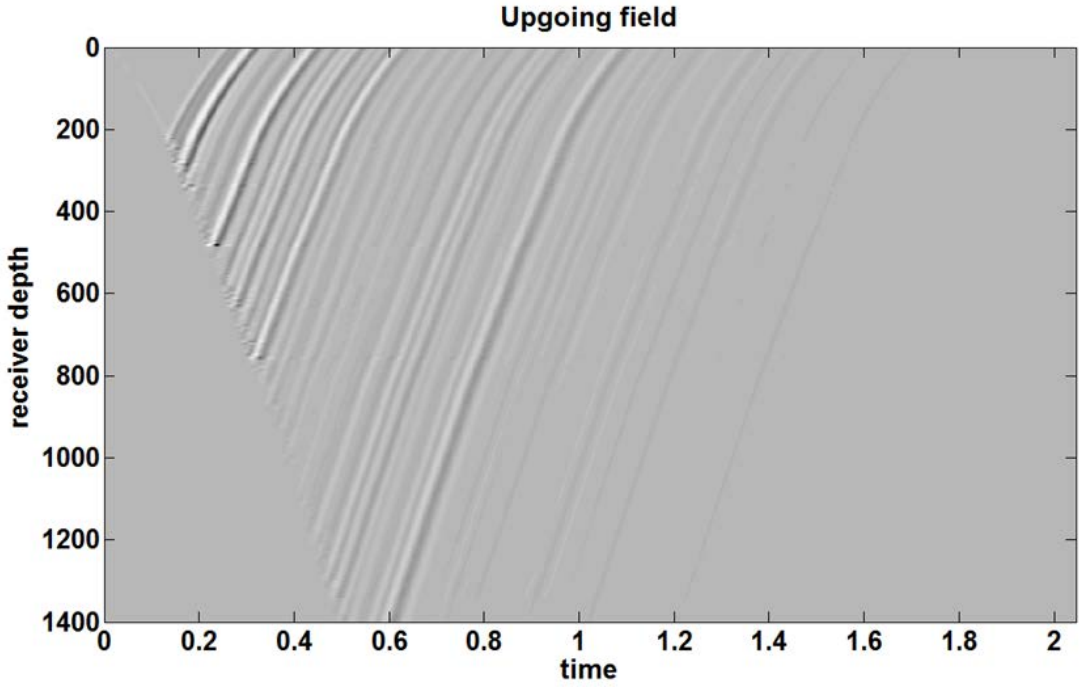


Figure 13: The upgoing field from Figure 11.

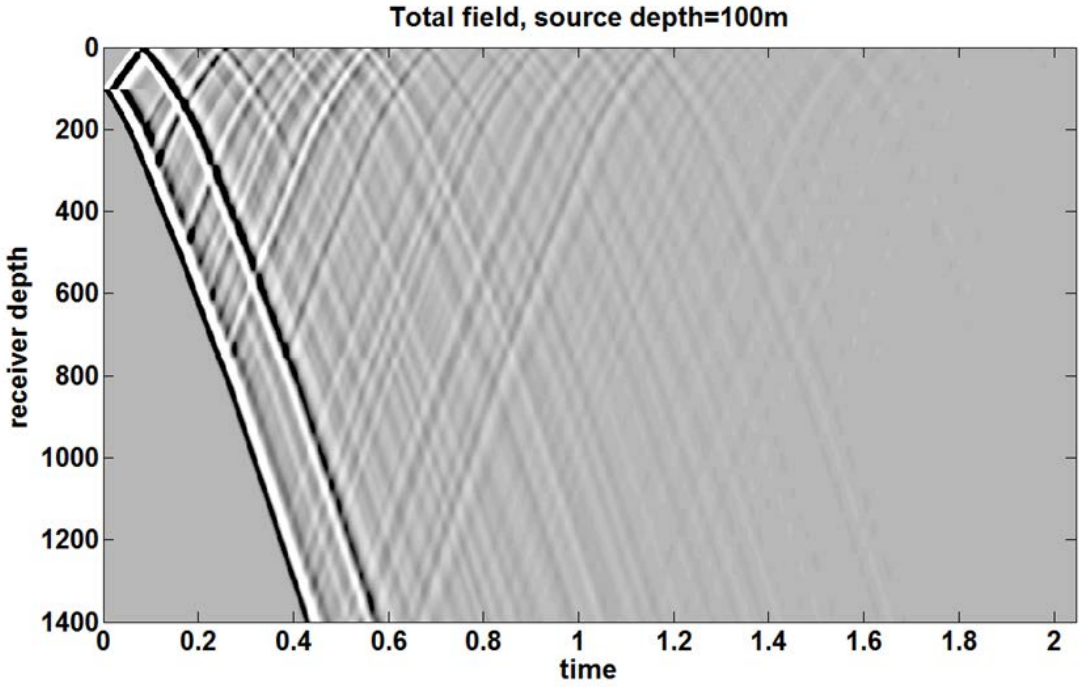


Figure 14: The total displacement field for the model of Figure 10 when the source is at a depth of 100m. Compare to Figure 11.

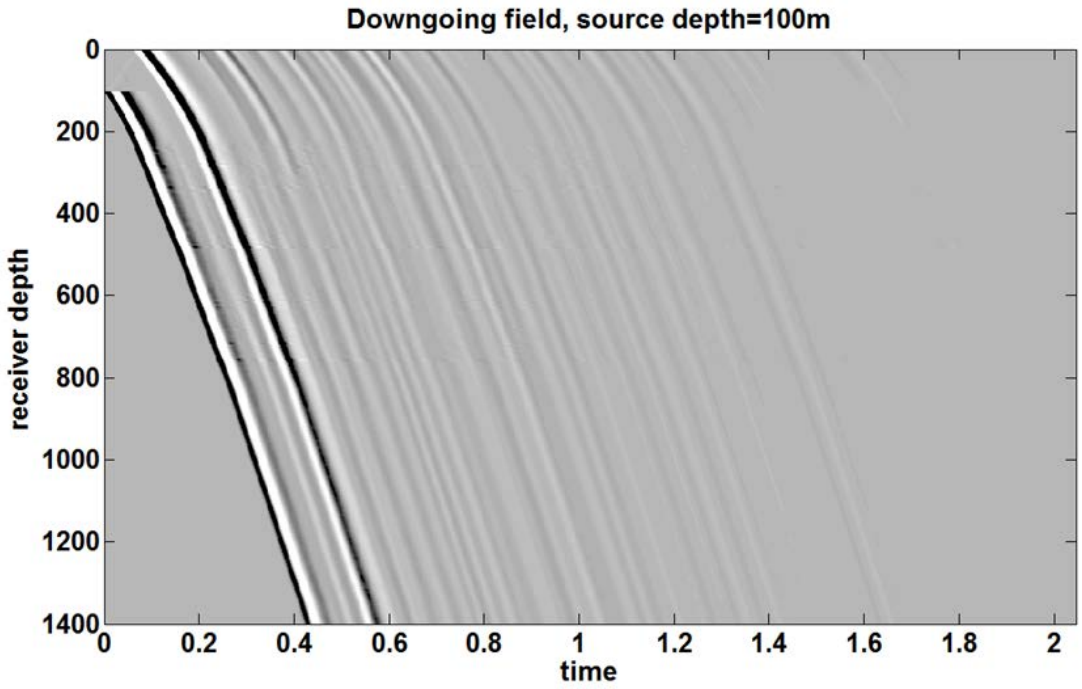


Figure 15: The downgoing field from the solution of Figure 14.

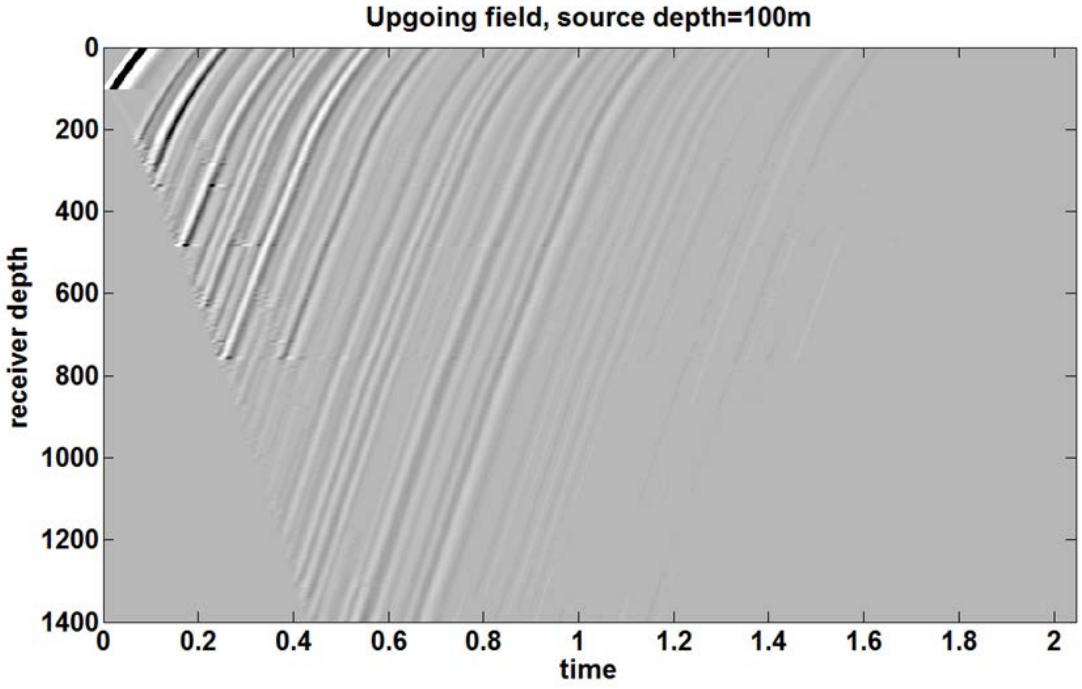


Figure 16: The upgoing field from the solution of Figure 14.

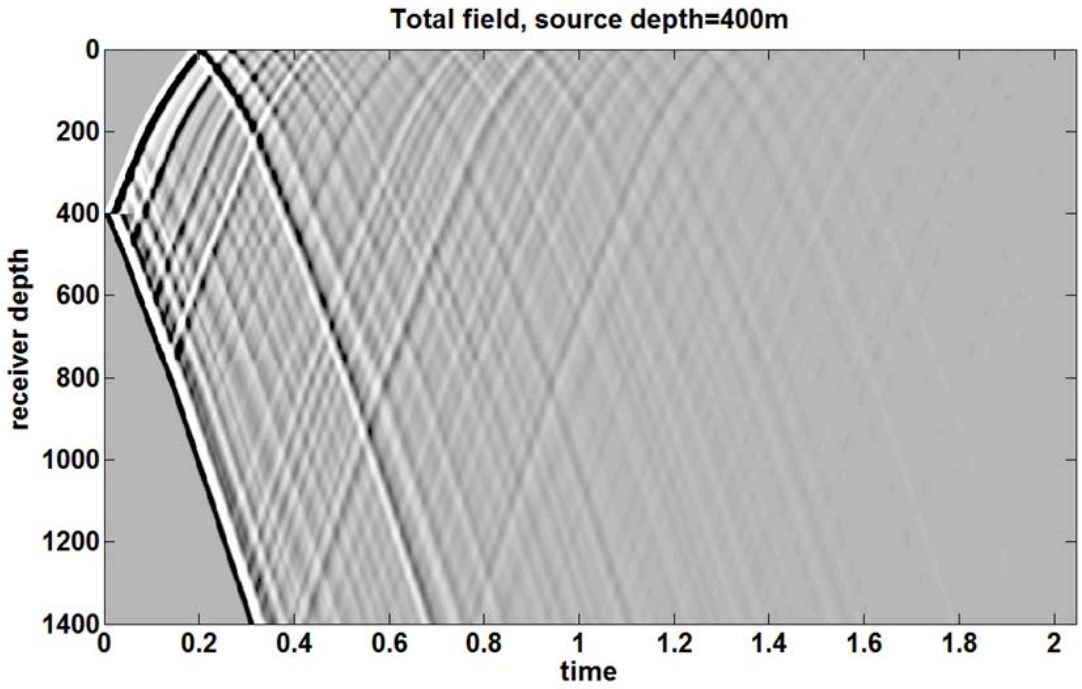


Figure 17: The total displacement field for the model of Figure 10 and with a source depth of 400m. Compare to Figures 14 and 11.

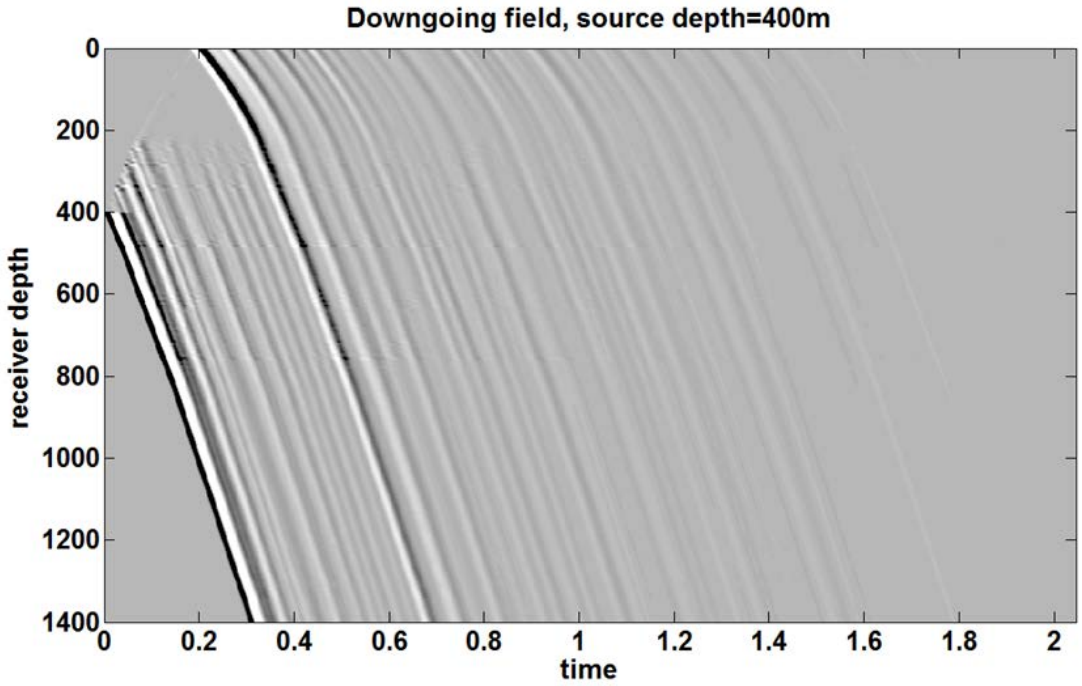


Figure 18: The downgoing field from the solution of Figure 17.

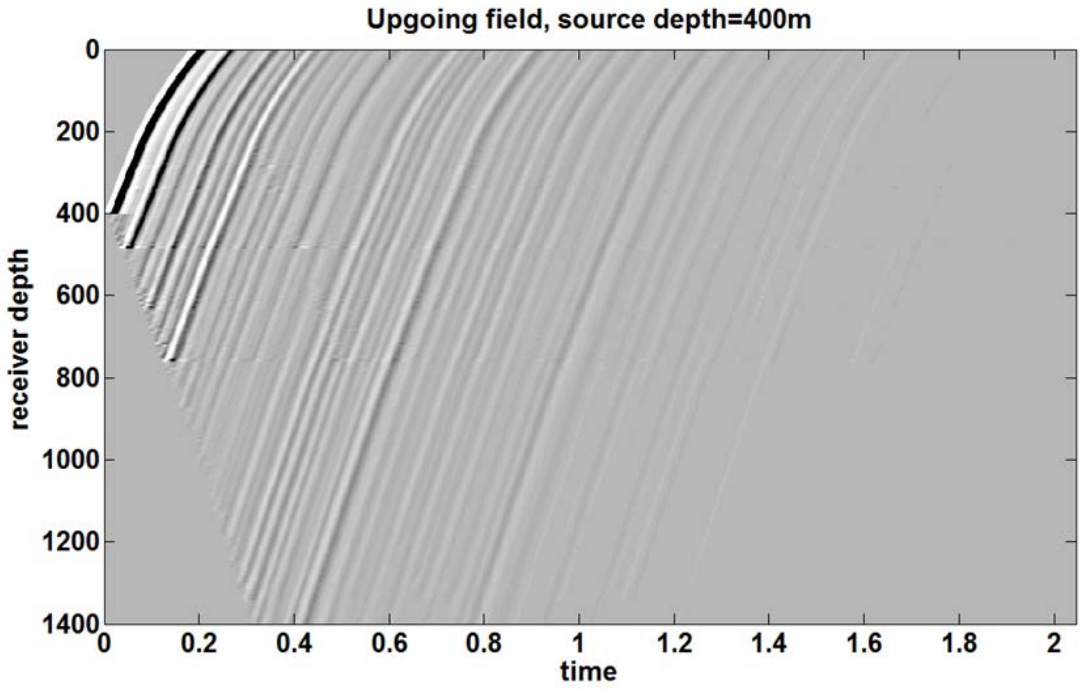


Figure 19: The upgoing field from the solution of Figure 17.

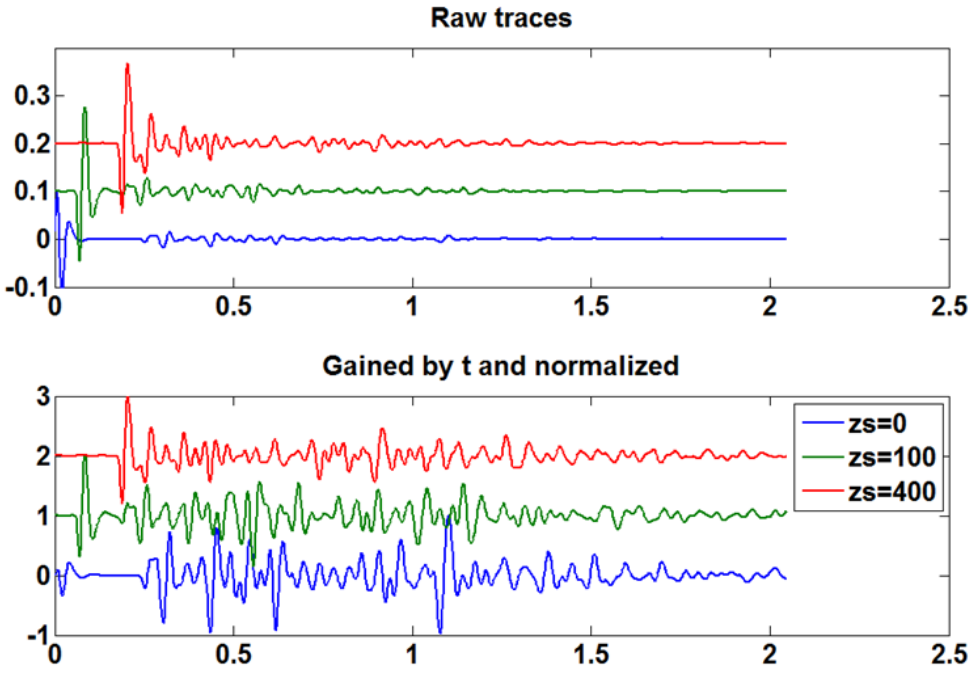


Figure 20: The surface seismograms from the receiver at z=0 in Figures 11, 14, and 17. In the upper figure the traces are shown in raw amplitude while in the lower figure the traces have been gained by multiplication by t (time) and normalized to 1.

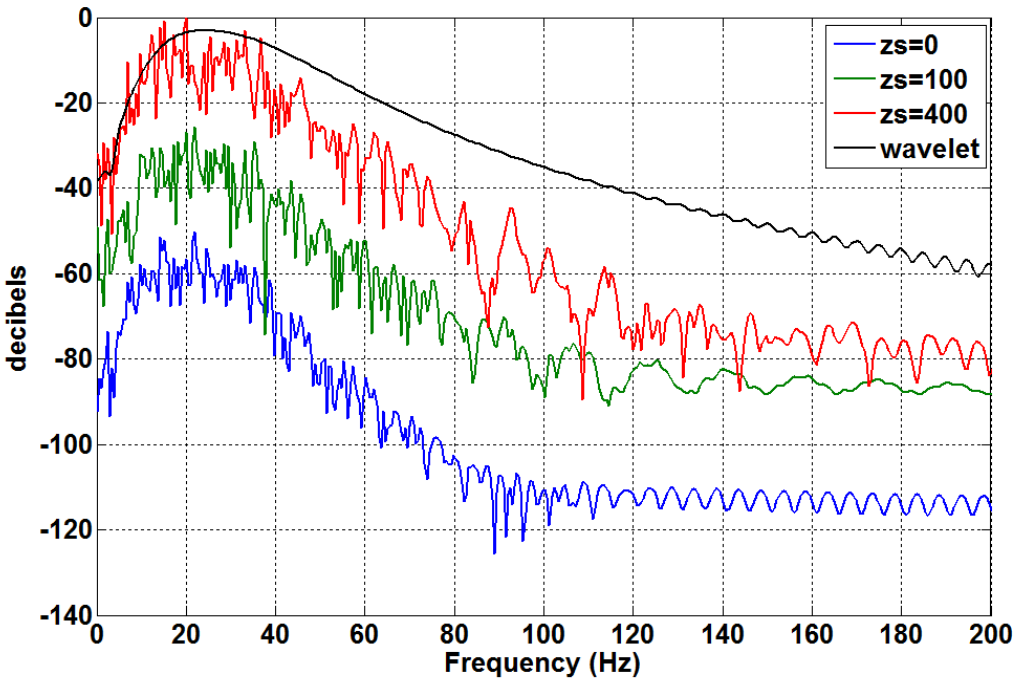


Figure 21: Spectra of the three gained and normalized surface seismograms from the lower panel of Figure 20. Also shown is the spectrum of the source wavelet. The spectra have been shifted vertically to ease comparison as they would otherwise plot on top of each other.

The z=0 receiver in these simulations is a prediction of the expected recording at the earth's surface. The three z=0 seismograms, corresponding to the receiver at zero depth in Figures 11, 14, and 17, are shown in Figure 20. The raw seismograms show strong decay with time due to a combination of transmission losses and $Q$ attenuation. It is also apparent that the surface source produces the weakest seismogram due to increased $Q$ and transmission effects. In the lower panel the seismograms have been gained by simple multiplication by t (i.e. $s_g(t) = t\,s(t)$) and normalized to 1, to facilitate comparison. In Figure 21 are the amplitude spectra of these gained seismograms together with the amplitude spectrum of the source wavelet. There is stronger decay with increasing frequency in the seismograms than is in the source wavelet and this is due to the cumulative effect of the $Q$ model. We can also see that the spectra apparently flatten after about 60db of attenuation (measured from the maximum of each spectrum) which may indicate the dynamic range for this modelling. This point needs further investigation. At this stage, it is also not obvious that the $Q$ attenuation is producing accurate results. Elsewhere in this report (Margrave 2014) it is shown in great detail that the attenuation is accurate and believable and that the stratigraphic filtering of O'Doherty and Anstey (1971) is produced by this algorithm.

## CONCLUSIONS

A propagator method for the construction of synthetic seismograms including constant-$Q$ attenuation and all possible multiples has been described and implemented in Matlab code released to sponsors. This source code is well documented and can easily be

translated into any other language. Although previously described in the literature, extensions to arbitrary source depth and to turn internal multiples, surface multiples, and attenuation off and on are described. As described, the method has the ability to model either displacement or pressure recordings which have opposite polarity effects on reflection. Examples were presented for a simple conceptual model and for a model derived from well-log measurements. The resulting synthetic VSP's are shown to be correct and to have high fidelity.

## ACKNOWLEDGEMENTS

We thank the sponsors of CREWES for their support. We also gratefully acknowledge support from NSERC (Natural Science and Engineering Research Council of Canada) via two grants: CRDPJ 379744-08 and RGPIN 217032-2013.

## REFERENCES

Aki, K, and P.G. Richards, 2002, Quantitative Seismology, University Science Books.

Emmerich, H. and M. Korn, 1987, Incorporation of attenuation into time-domain computations of seismic wave fields. Geophysics, 52(9), pp. 1252–1264.

Barr. F. J. and J. I. Sanders, 1989, Attenuation of water-column reverberations using pressure and velocity detectors in a water-bottom cable. SEG Technical Program Expanded Abstracts 1989: pp. 653-656.

Ganley, D. C., 1981, A method for calculating synthetic seismograms which include the effects of absorption and dispersion, GEOPHYSICS Aug 1981, Vol. 46, No. 8, pp. 1100-1107.

Kjartansson, E, 1979, Constant Q-wave Propagation and Attenuation, Journal of Geophysical Research, **84**, 4737-4748.

Krebes, E. and G. Quiroga-Goode, 1994, A standard finite-difference scheme for the time-domain computation of anelastic wavefields. Geophysics, 59(2), pp. 290–296.

Margrave, G. F., 2014, Stratigraphic filtering and Q estimation, CREWES Research Report, Volume 26.

O'Doherty, R. F., and N. A. Anstey, 1971, Reflections on Amplitudes, Geophysical Prospecting, 19, pp. 430-458.